Temperature and Size Dependence of Antiferromagnetism in Mn Nanostructures

P. Sessi,[1] N. P. Guisinger,[2] J. R. Guest,[2] and M. Bode[2]

[1]*CNISM–Dipartimento di Fisica, Politecnico di Milano, I-20133 Milano, Italy*

[2]*Center for Nanoscale Materials, Argonne National Laboratory, Argonne, Illinois 60439, USA*

(Received 2 June 2009; published 13 October 2009)

We report on variable-temperature STM investigations of the spontaneous long-range magnetic order of Mn monolayer nanostructures epitaxially grown on stepped W(110). The measurements reveal that the onset of the antiferromagnetic order is closely related to the Mn nanostructure width along the [001] direction, with a decreasing Néel temperature as we move from a 2D toward a quasi-1D system. In contrast, lateral confinement along the $[1\bar{1}0]$ direction seems to play a less important role. The results are discussed in terms of anisotropic exchange coupling and of boundary effects, both potentially stabilizing long-range magnetic order in nanostructures confined in the $[1\bar{1}0]$ direction.

DOI: 10.1103/PhysRevLett.103.167201 PACS numbers: 75.70.Ak, 68.37.Ef

Driven by sensor and data storage applications of the exchange-bias effect [1] and heat-assisted magnetic recording [2], the temperature-dependent properties of low-dimensional and nanoscale magnetic particles have been of substantial recent interest. Low-dimensional *ferromagnets* have been in the focus of basic and applied research for several decades. The advent of commercially available ultrahigh vacuum (UHV) technology initiated studies of two-dimensional (2D) magnetic films [3,4]. Further advancements of self-organized [5] and lithography-based preparation methods as well as the development of refined analysis tools also allowed the investigation of properties of one- [6–8] and zero-dimensional magnets [9–11] leading to a quite thorough understanding of ferromagnetism at low dimensions [12].

In contrast, much less is known about the properties of low-dimensional *antiferromagnets* (for a recent review, see Ref. [13]). The main reason for this deficiency is that the magnetic moments of antiferromagnets cancel. The resulting lack of net magnetization essentially renders spatially averaging techniques unsuitable for studying their magnetic properties. This shortcoming can be overcome by experimental methods which allow for atomic spin resolution imaging, such as spin-polarized scanning tunneling microscopy [14] or exchange force microscopy [15]. Although some progress has been made in imaging the static magnetic order in collinear [16] and noncollinear antiferromagnetic [17,18] spin structures, the dependence of magnetic phase transitions on the sample's reduced dimensionality, which are more sensitive to statistical fluctuations, remain largely unexplored as spin-resolved atomic-resolution STM studies at variable temperatures are extremely challenging, especially if the subject also requires the imaging of extended areas.

We have bypassed this issue by making use of the particular electronic structure of the Mn monolayer on W (110), which offers a convenient link between its magnetic and spin-averaged electronic structure. It has recently been revealed by spin-polarized STM and *ab initio* density-functional theory (DFT) that at low temperature the Mn monolayer—driven by the Dzyaloshinskii–Moriya interaction—forms a cycloidal antiferromagnetic spin spiral as schematically represented in Fig. 1 [18]. While Mn spins of individual [001] rows are aligned parallel, adjacent [001] rows exhibit an almost antiparallel but slightly canted order. This canting angle, which amounts to $\approx 7°$ between adjacent [001] rows and leads to a magnetic periodicity of about 12 nm, results in a static cycloidal modulation of the spin structure with periodically alternating in-plane and out-of-plane magnetized regions (see Fig. 1). Spin-orbit coupling leads to enhanced (reduced) electronic local density of states (LDOS) over in-plane (out-of-plane) magnetized regions which can be detected even with nonmagnetic tips [19]. By making use of this so-called spin-orbit contrast (SOC) two benefits are exploited: (i) The existence of the spin spiral can be discerned without the need of a magnetic tip and (ii) it allows bridging the gap between atomic scale spin order and mesoscopic surface features like the surface's step edge and terrace structure because the magnetic superstructure manifests itself on a larger length scale (6 nm).

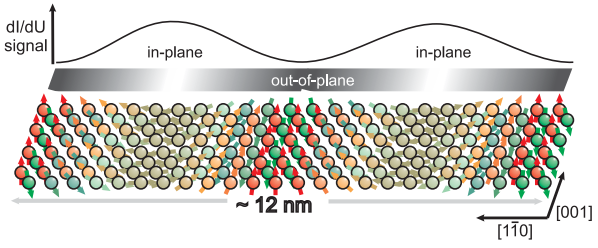

FIG. 1 (color online). (bottom panel) Schematic spin structure of the Mn monolayer on W(110). Nearest neighbor spins are slightly canted resulting in a cycloidal spin spiral with alternating out-of-plane and in-plane regions which repeat with a period of about 6 nm. (top) Spin-orbit coupling leads to an enhanced (reduced) LDOS over in-plane (out-of-plane) magnetized regions which can be detected with nonmagnetic tips.

In this Letter we report on a variable-temperature STM study of the spontaneous long-range magnetic order of Mn monolayer nanostructures epitaxially grown on W(110). The nanostructures are prepared by deposition on a stepped substrate. In doing so the step accumulation of W(110) is utilized to obtain different terrace widths thereby allowing us to study the effects of lateral confinement within a single experimental run. Our data reveal that the onset of the antiferromagnetic order is closely related to the Mn nanostructure width along the [001] direction, with a decreasing Néel temperature as we move from a 2D toward a quasi-1D system. In contrast, lateral confinement along the $[1\bar{1}0]$ direction plays a less important role as no obvious correlation to the temperature-dependent ordering can be observed.

The experiments have been performed in a commercial variable-temperature UHV-STM with separate chambers for sample preparation and surface analysis. The W(110) substrate preparation was described elsewhere [21]. Mn was evaporated at a deposition rate of approximately 1 atomic layer (AL) per minute. In order to achieve step-flow growth, the substrate was held at elevated temperature ($T \approx 500$ K) during Mn deposition. Constant current images and differential conductance dI/dU maps have been recorded simultaneously by means of a lock-in technique.

Figure 2 shows (a) the topography and (b) the dI/dU map of 0.95 AL Mn on W(110) measured with an Fe-coated W tip with the inset showing a higher resolution topographic image of the Mn monolayer. While the topography overview image in Fig. 2(a) is governed by three atomically flat terraces which are separated by two monatomic step edges, the high resolution inset, owing to the tip magnetic sensitivity, sheds light on the magnetic structure at the atomic level revealing atomic scale bright and dark stripes running along the [001] direction. The contrast of these stripes is not constant but is modulated with a period of about 6 nm, thereby confirming earlier reports on a cycloidal antiferromagnetic spin spiral with alternating out-of-plane and in-plane antiferromagnetic order [18]. As a result of the above mentioned SOC, the Mn covered areas in Fig. 2(b) reveal a periodic modulation of the dI/dU signal with stripes running along the [001] direction. Considering that the Fe-coated tip is in-plane sensitive, it is possible to match the minima of the magnetic corrugation (inset) with the minima of the local density of states in the dI/dU signal [Fig. 2(b)]. Figure 2(c) shows an average Fourier transform (FFT) of line sections taken along the $[1\bar{1}0]$ direction in Fig. 2(b). The pronounced peak at approximately 0.16 nm^{-1} corresponds to the magnetic modulation period of the Mn monolayer of about 6 nm. This Fourier analysis method of STM data was found to be very sensitive to the existence of magnetic order and will be used to detect the presence of long-range cycloidal antiferromagnetic order in the following study of its temperature and size dependence.

Figure 3(a) shows the topography of 0.85 AL Mn/W(110). All W(110) step edges run approximately along

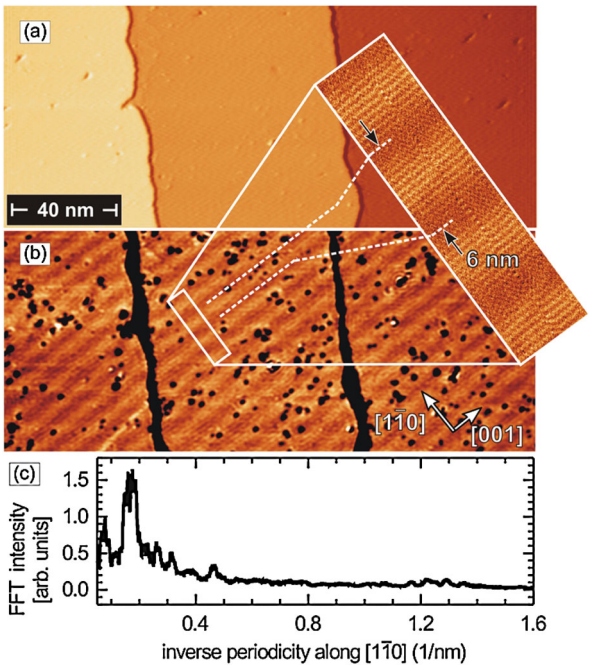

FIG. 2 (color online). (a) Topography and (b) differential conductance dI/dU of 0.95 AL Mn/W(110) ($T = 40$ K, $U = +150$ mV). At this bias voltage out-of-plane and in-plane regions of the antiferromagnetic spin spiral can be distinguished because of a weak spin-orbit contrast (SOC) in the spin-averaged LDOS. High resolution topographic data taken with an in-plane sensitive Fe-coated tip show the atomically resolved spin structure (inset). (c) The FFT spectrum of (b) along the $[1\bar{1}0]$ direction exhibits a peak at the inverse periodicity of the SOC, i.e., 0.16 nm^{-1}.

the $[1\bar{1}0]$ direction. While the average terrace width on our substrate is $\approx$80 nm, it varies substantially at different locations of the crystal surface because of local step accumulation. Within the area shown here, terrace widths from 125 nm (A) to 20 nm (C) were found. The terrace width was found to influence the morphology of the Mn film. In addition to limiting the width of the Mn nanostructure (along the [001] direction), the terrace width also has a significant impact on the Mn film morphology in the direction *along* the step edges (along the $[1\bar{1}0]$ direction). This can be seen by comparing the morphology of the Mn film on the terraces labeled A and C in Fig. 3(a). The Mn film on the narrow terrace C has a very low edge roughness, is a perfectly continuous ribbon and—as far as we can tell—effectively infinitely long. In contrast, the Mn film grown on terrace A exhibits trenches perpendicular to the step edges. These different growth modes might be caused by anisotropic diffusion barriers [22,23]. Note that the film on broad terraces such as A is discontinuous in both directions, perpendicular to and along the step edges, and that the size of some patches along the $[1\bar{1}0]$ direction are comparable with the [001] width of the continuous Mn monolayer ribbon on terrace C. As we will point out below these different morphologies lead to different magnetic properties.

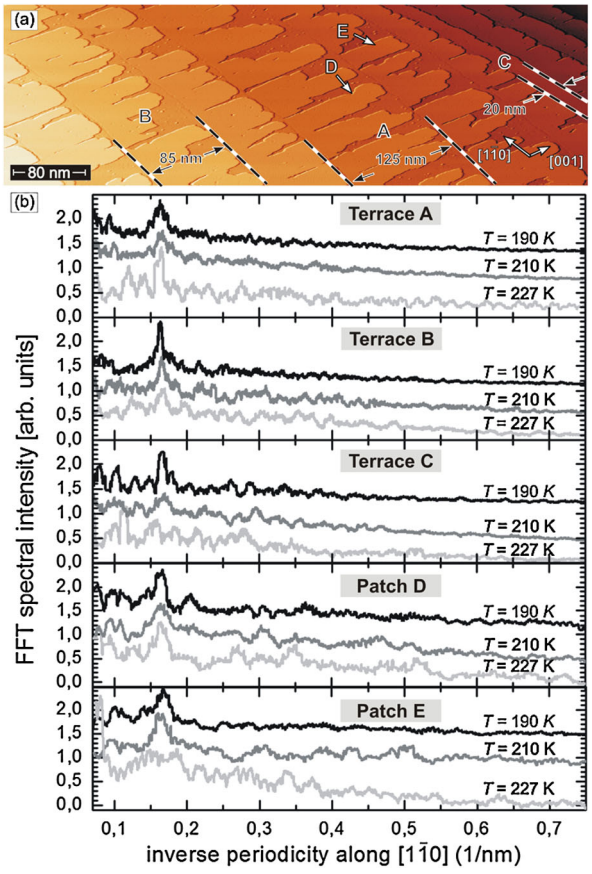

FIG. 3 (color online). (a) Topography of 0.85 AL of Mn on stepped W(110). The terrace width which amounts to 80 nm in average (e.g., terrace B) varies between 130 nm (A) and 20 nm (C). (b) Temperature-dependent FFT spectra of dI/dU line sections ($U = +150$ mV) taken along the [1$\bar{1}$0] direction. The peak at 0.16 nm^{-1} is characteristic for cycloidal magnetic order. While it remains visible up to 227 K on the wide terraces A and B and even on the patches D and E the peak vanishes on the narrow terrace C indicating a magnetic ordering temperature below 227 K.

In order to understand the influence of lateral confinement on the onset of antiferromagnetism in Mn nanostructures, we collected a temperature series of differential conductance dI/dU maps at the same location. For quantification the dI/dU maps have been analyzed by Fourier transformation of line sections along the [1$\bar{1}$0] direction, i.e., the direction perpendicular to the stripes. The results for terraces A, B, and C and the patches D and E are reported in Fig. 3(b) for three temperatures.

At the lowest temperature shown here, $T = 190$ K, all three terraces exhibit a clear peak centered at about 0.16 nm^{-1} that corresponds to the 6 nm modulation. With increasing sample temperature the general trend of a decreasing peak intensity is observed. Quantitatively, however, the reduction is quite different and was found to depend on the dimensions of the Mn nanostructure along the [001] direction, i.e., the width of the terrace. While a partial reduction of the spectral intensity was observed between 190 and 227 K for terraces A and B, the peak intensity vanishes completely within the noise level for the narrowest Mn ribbon on terrace C.

For further quantitative analysis and under the assumption of noise dominated by thermal fluctuations, we fitted the peaks of terraces A-C shown in Fig. 3(b) and of six other terraces after background subtraction. Data taken on nine terraces in Fig. 3(a) are summarized in Fig. 4 with the inset showing the detailed results for terraces A, B, and C. The compilation shows that, similar to experiments on ultrathin ferromagnetic films deposited on differently stepped substrates [24,25], the magnetic ordering temperature of Mn monolayer nanostructures is width dependent along the [001] direction.

In contrast, geometrical confinement in the [1$\bar{1}$0] direction does not seem to influence the magnetic ordering temperature as evidenced by FFT spectra taken on the highly discontinuous terrace A. This assumption is confirmed by data taken from patch D which is connected by a narrow monolayer bridge to an adjacent patch and even the well-separated patch E in Fig. 3(a). The width of both patches ([1$\bar{1}$0] direction) amounts to 24 ± 2 nm which is comparable to the Mn width on terrace C. While a similar confinement along the [001] direction on terrace C leads to strong reduction of the magnetic ordering temperature [cf. Fig. 4], the Fourier spectra of both patches [two bottom panels of Fig. 3(b)] show a broadened but nonvanishing peak intensity thereby indicating that they maintain their cycloidal antiferromagnetic order well above 227 K.

One possible explanation for the observed behavior might be anisotropic exchange coupling in the Mn monolayer. DFT calculations have shown that the spin stiffness of homogeneous spin spirals in the Mn monolayer on W(110) is higher along the [1$\bar{1}$0] than along the [001] direction, potentially causing the magnetic order along

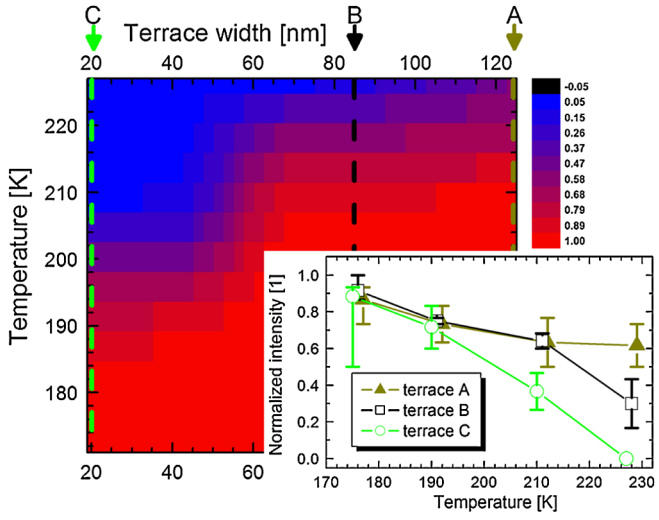

FIG. 4 (color online). Color-coded peak intensity at an inverse periodicity of 0.16 nm^{-1} as found on nine terraces in Fig. 3. The inset shows the peak intensity found on terraces A, B, and C after normalization at 40 K.

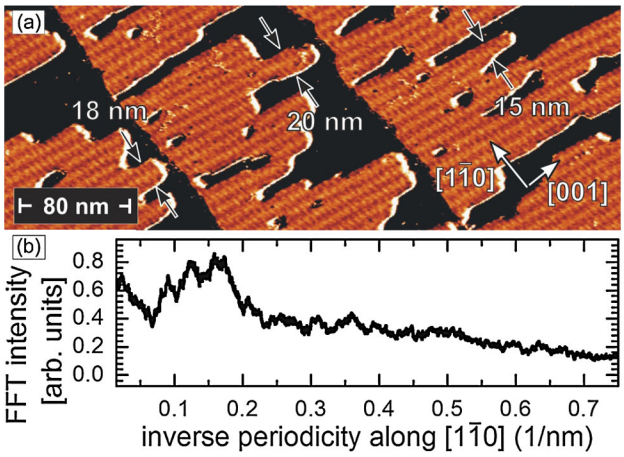

FIG. 5 (color online). (a) dI/dU map showing the spin-orbit contrast (SOC) characteristic for long-range antiferromagnetic order ($T = 40$ K, $U = +150$ mV). Fingerlike structures with dimensions down to below 15 nm along the $[1\bar{1}0]$ direction can be seen. Pinning of the minimum of the SOC (out-of-plane antiferromagnetic regions) can be observed at the edge of the fingers. (b) FFT of line sections taken along the $[1\bar{1}0]$ direction. The peak is much broader than in comparable data taken on terraces which are quasi-infinite along the $[1\bar{1}0]$ direction [cf. Fig. 3(b)].

the [001] direction to be more susceptible to thermal fluctuations (see Fig. 4 in Ref. [18]). Alternatively, magnetic order in the $[1\bar{1}0]$ direction might result from boundary effects of the cycloidal spin spiral locked into a geometrically confined arrangement. The existence of boundary effects is demonstrated in Fig. 5 which shows a dI/dU map taken at $U = +150$ mV dominated by the spin-orbit contrast indicating magnetic order. The topography of this sample exhibits patches along the $[1\bar{1}0]$ direction with a minimal width well below 20 nm. In spite of this narrow confinement the SOC can be observed to the very end of each structure. More importantly, the minimum of the SOC which corresponds to out-of-plane antiferromagnetic regions as shown in Fig. 2 is always found at the Mn edges running along the [001] direction. Since, however, the Mn width is not necessarily a multiple of the spin spiral periodicity, the boundary condition of a perpendicular spin configuration at Mn edges leads to a significant variation of periodicity. This can be seen in the strongly broadened peak in the FFT of line sections taken in the $[1\bar{1}0]$ direction, shown in inset of Fig. 5.

In summary, we have performed a variable-temperature STM study of the spontaneous long-range magnetic order in antiferromagnetic nanostructures. The measurements reveal that the onset of the antiferromagnetic order is closely related to the structural width along the [001] direction, with a decreasing Néel temperature as we move from a 2D toward a quasi-1D system. In contrast, lateral confinement along the $[1\bar{1}0]$ direction seems to play a less important role with no obvious correlation to the temperature-dependent ordering. The results are discussed in terms of anisotropic exchange coupling and of boundary effects, both potentially stabilize the long-range magnetic order when the reduction of dimensionality occurs in the $[1\bar{1}0]$ direction.

Use of the Center for Nanoscale Materials was supported by the U. S. Department of Energy, Office of Science, Office of Basic Energy Sciences, under Contract No. DE-AC02-06CH11357.

[1] F. Radu and H. Zabel, *Springer Tracts in Modern Physics* (Springer, Berlin, 2008), Vol. 227, pp. 97–184.
[2] M. H. Kryder *et al.*, Proc. IEEE **96**, 1810 (2008).
[3] G. A. Prinz, Phys. Rev. Lett. **54**, 1051 (1985).
[4] U. Gradmann, in *Handbook of Magnetic Materials*, edited by K. H. J. Buschow (Elsevier, Amsterdam, 1993).
[5] O. Fruchart, C.R. Physique **6**, 61 (2005).
[6] J. Shen *et al.*, Phys. Rev. B **56**, 2340 (1997).
[7] J. Hauschild, H. J. Elmers, and U. Gradmann, Phys. Rev. B **57**, R677 (1998).
[8] P. Gambardella, J. Phys. Condens. Matter **15**, S2533 (2003).
[9] O. Fruchart *et al.*, Phys. Rev. Lett. **83**, 2769 (1999).
[10] P. Gambardella *et al.*, Science **300**, 1130 (2003).
[11] F. Meier *et al.*, Science **320**, 82 (2008).
[12] S. D. Bader, Rev. Mod. Phys. **78**, 1 (2006).
[13] S. Mørup *et al.*, J. Phys. Condens. Matter **19**, 213202 (2007).
[14] M. Bode, Rep. Prog. Phys. **66**, 523 (2003).
[15] U. Kaiser, A. Schwarz, and R. Wiesendanger, Nature (London) **446**, 522 (2007).
[16] A. Kubetzka *et al.*, Phys. Rev. Lett. **94**, 087204 (2005).
[17] M. Bode *et al.*, Nature Mater. **5**, 477 (2006).
[18] M. Bode *et al.*, Nature (London) **447**, 190 (2007).
[19] Similar to recent observations on the Fe double layer on the same substrate [20], the high atomic number of W leads to strong spin-orbit interaction effects in Mn. Together with the uniaxial anisotropy of a bcc(110) surface this results in distinct magnetization-orientation–dependent variation of the spin-averaged electronic structure [20], i.e., a local density of states which is slightly enhanced over in-plane regions compared to out-of-plane antiferromagnetic regions (see top panel of Fig. 1).
[20] M. Bode *et al.*, J. Phys. Condens. Matter **15**, S679 (2003).
[21] M. Bode *et al.*, Surf. Sci. **601**, 3308 (2007).
[22] S. Dennler and J. Hafner, Phys. Rev. B **72**, 214414 (2005).
[23] See EPAPS Document No. E-PRLTAO-103-005944 for supplementary information on the growth of Mn monolayer on terraces with different step edge orientations. For more information on EPAPS, see http://www.aip.org/pubservs/epaps.html.
[24] H. J. Elmers, J. Hauschild, and U. Gradmann, J. Magn. Magn. Mater. **177–181**, 827 (1998).
[25] H. J. Elmers, J. Hauschild, and U. Gradmann, J. Magn. Magn. Mater. **221**, 219 (2000).